Formic Acid as a Dopant for Atmospheric Pressure Chemical Ionisation (APCI) for Negative Polarity of Ion Mobility Spectrometry and Mass Spectrometry

Vahideh Ilbeigi[1,*], Younes Valadbeigi[2,*], Ladislav Moravsky[1] and Štefan Matejčík[1,*]

[1]Department of Experimental Physics, Faculty of Mathematics, Physics and Informatics, Comenius University in Bratislava, Mlynská dolina F2, 84248 Bratislava, Slovakia.

[2]Department of Chemistry, Faculty of Science, Imam Khomeini International University, Qazvin, Iran.

Emails: vahideh.ilbeigi@fmph.uniba.sk; stefan.matejcik@fmph.uniba.sk

Abstract

Formic acid (FA) is introduced as a potent dopant for atmospheric pressure chemical ionization (APCI) for ion mobility spectrometry (IMS) and mass spectrometry (MS). The mechanism of chemical ionization with FA dopant was studied in the negative polarity using a corona discharge (CD) - IMS - MS technique (CD-IM-MS) in air. Standard reactant ions of the negative polarity present in air are $O_2^-\cdot(CO_2)_n\cdot(H_2O)_m$ (m=0,1 and n=1,2) clusters. Introduction of FA dopant resulted in production of $HCOO^-\cdot FA$ reactant ions. The effect of FA dopant on APCI of different classes of compounds was investigated, including plant hormones, pesticides, acidic drugs, and explosives. FA dopant APCI resulted in the deprotonation and/or adduct ion formation, $[M-H]^-$ and $[M+HCOO]^-$, respectively. Supporting density functional theory (DFT) calculations showed that ionization mechanism depended on the gas phase acidity of the compounds. FA dopant APCI led to the improvement of detection sensitivity, suppression of fragmentation, and changes in the ion mobilities of the analyte ions, for analytes with suitable molecular structure and gas acidity.

1. Introduction

Ion mobility spectrometry (IMS) is a gas phase separation technique with a growing number of applications in many fields of science and technology. In IMS, ions travel through an inert drift gas environment under the action of an electric field and their separation is achieved due to differences in mass and structure of the ions and due to differences in collisional interactions of the ions with the drift gas molecules.[1] Modern commercial (low pressure) IMS instruments, combined with high resolution mass spectrometry (HRMS) have been coupled with gas chromatography and liquid chromatography (LC) to provide an additional separation dimension for analytes based on their collisional cross section (CCS).[2] On the other hand, low cost stand-alone (high pressure) IMS instruments are increasingly popular due to their simple usage, high sensitivity, fast and real-time analysis. These instruments have wide-ranging applications in the detection of volatile organic compounds (VOC),[3] explosives,[4,5] chemical agents,[6] abused drugs,[7,8] food ingredients,[9] and breath analysis.[10,11] The ionization sources of these instruments are mainly based on the atmospheric pressure chemical ionization (APCI) method, with primary ion sources such as corona discharge (CD) or ^{63}Ni radioactive sources.[1]

APCI-CD ionization sources operate in positive and negative polarities for the detection of cations and anions, respectively. The ionization mechanism in APCI is based on the ionization of the analyte via reaction with the reactant ions (RI) produced by the CD.[1] Different types of RIs can be generated in the positive and negative polarities, hence, a variety of ionization mechanisms can act on the analytes in the gas phase. The nature of the RIs generated in CD depends on the composition of the gas and on the design of the ion source. In the positive mode (with air as the drift gas) $H_3O^+\cdot(H_2O)_n$, $NH_4^+\cdot(H_2O)_m$ and $NO^+\cdot(H_2O)_k$(all or some of them, m,n,k=0,1,2,3...) have been reported as the RIs and the ionization of the analytes (M) proceeds via protonation, cation attachment, charge transfer and hydride abstraction to produce product ions $[M+H]^+$, $[M+RI]^+$, $[M]^{\cdot+}$, and $[M-H]^+$, respectively.[12-14] Most frequent RIs in the negative mode (also in air) are $O_2^{-\cdot}(H_2O)_x\cdot(CO_2)_y$,

$CO_3^-\cdot(H_2O)_m$, and $NO_x^-\cdot(H_2O)_n$ which ionize the analyte by deprotonation, charge transfer, and anion attachment and produce product ions $[M-H]^-$, $[M]^{\bullet-}$, and $[M+RI]^-$, respectively.[15-17] For efficient ionization of analytes in APCI, the selection of ion source polarity (positive or negative) and RIs strongly depends on the structure, and chemical and physical properties of the analyte, such as basicity, acidity, ionization energy and electron affinity.[18] Many analytes can be ionized via more than one ionization pathway, or the ionization may produce fragments, resulting in complex IM spectra with several (often overlapping) peaks.[14] Additionally, some analytes are not ionized by standard RIs, or the ionization efficiency is weak, resulting in weak response in both positive and negative modes.

To overcome these issues, a range of modifier or dopant gases are introduced into the CD ion source, to convert the standard RIs to dopant RIs and thus change the ionization mechanism. Such dopants are used to improve the sensitivity and selectivity of the ionization process, modify the nature of the analyte ions (the ion mobilities of the analyte ions) to reduce the IMS peak overlapping, and even to achieve conformer and chiral separation.[19-28]

In the positive polarity, the most common dopant gases are NH_3, NO, and NO_2, which produce $NH_4^+\cdot(H_2O)_m$ and $NO^+\cdot(H_2O)_n$ RIs.[25,29,30] As NH_3 has higher gas phase basicity than H_2O, ionization of analytes by $NH_4^+\cdot(H_2O)_m$ is more selective than that by $H_3O^+\cdot(H_2O)_m$so that only compounds with higher basicity than NH_3 are protonated.[21] However, compounds with basicity lower than NH_3 can also be ionized via ammonium attachment, $[M+NH_4]^+$, leading to IM-peak shift compared to ionization by H_3O^+ RIs.[29] Nitrogen oxides (NO and NO_2) dopants are used for the formation of $NO^+\cdot(H_2O)_k$ in the positive polarity and ionization of aromatic compounds, such as benzene, toluene, and xylene via charge transfer and NO^+ attachment.[30]

In the negative polarity, the O_2^--based RIs ($O_2^-.(H_2O)_n$, $O_2^-.(CO_2)_m(H_2O)_n$)are strong bases in the gas phase,[31,32]hence, they ionize analytes with a wide range of acidities via deprotonation. However, O_2^- attachment is likewise a possible ionization pathway for analytes with low acidity in the gas phase.[33-35] To improve the selectivity, halogen-containing compounds such as halomethanes (mainly $CHCl_3$, CCl_4, $CHBr_3$) are used as dopants,

resulting in the production of Cl^- and Br^- RIs with lower gas phase basicity than O_2^-.[36] In addition, Cl^- and Br^- can improve the resolution and, in case of ionization of analytes via anion attachment, produce $[M+Cl]^-$ and $[M+Br]^-$ leading to IMS peak shift.[37]

In this work, we introduce formic acid (FA) as a potent dopant for APCI ionization in the negative polarity, which can be applied to IMS and MS techniques. To assess the efficiency of this dopant, ionization of several analytes including plant hormones, drugs, explosives, and pesticides was investigated with and without FA dopant. To understand the IMS spectra, MS data were used to study the ionization mechanism of these compounds in the presence of FA dopant and the experimental observations were supported by density functional theory calculations of the RIs, analytes, and product ions, including the deprotonated species and the adducts with FA.

2. Experimental

2.1 Instrumentation

The CD-IMS-MS system used in this work was equipped with a point-to-plane CD-APCI ionization source operating in both positive and negative modes. The CD-IMS-MS is an in-situ manufactured instrument, constructed at the Department of Experimental Physics of Comenius University in Slovakia. A detailed description of the instrument can be found elsewhere.[38]The IMS drift tube operates at subambient pressure (600 mbar) and temperature of 80 ± 2 °C (temperature of the drift gas at exit), with a Faraday cup as the IMS detector at the end of the drift tube. In order to investigate the effect of the gas temperature, the measurements were also carried out at the elevated drift temperature of 120 °C for some of the compounds. The flow rate of the drift gas (purified ambient air) was 600 mL/min. A voltage of 8 kV was applied to the whole IMS cell (12.5 cm), to provide a drift field of 640 V/cm. The CD was supplied by a potential difference of 3 kV between the needle and the planar electrode. The IMS tube was connected to a differential pumping system through a 100 μm pinhole. The vacuum system consists of three chambers: the pressure of the first

chamber was reduced to 0.1 mbar using two rotary pumps, the pressures of the second and third chambers were 10^{-5} and 5×10^{-6} mbar, respectively, provided by turbomolecular pumps. The length of the linear time-of-flight MS was 54.7 cm with internal pressure of 10^{-5}mbar. A multichannel plate (MCP) was used as a detector for MS in the ion counting mode.

2.2 Materials and method

Indole-3-acetic acid (IAA, analytical standard, 98%), indole-3-propionic acid (IPA, 99%), indole-3-butyric acid (IBA, 99%), salicylic acid (SA, 99%),6-Benzylaminopurine (BAP,99%), kinetin (99%), Adenine (99%), 4-Chloro-2-methylphenoxyacetic acid, (MCPA, 95%), methanol (99.9%) were commercially obtained from Sigma-Aldrich, and formic acid (99.9%) was likewise purchased from Honeywell. TNT and RDX were procured from Slovak Department of Defense, with purity up to 99%. Naproxen (2-(6-methoxynaphthalen-2-yl) propanoic acid) and aspirin (2-acetyloxybenzoic acid) were purchased from Pars Darou Company, Iran.

Stock solutions of the analytes were prepared in methanol. For each measurement, 1 µl of the sample was injected into the injection port (200°C) and the vaporized sample was subsequently transported to the ionization region using a carrier gas (dried air) with a flow rate of 50 ml/min. The calibration curves were obtained for all compounds with and without FA dopant to obtain the practical limit of quantitation (LOQ). Limits of detection (LODs) were considered as LOQ/3. Head space of formic acid (FA) as a dopant was injected into the ionization region by dried air with flow rate of 5 ml min^{-1}. The schematic representation of the experimental set-up for the measurements with FA dopant is shown in Figure S1.

Purified dry ambient air was generated by MaSaTech s.r.o,(Slovakia) air generator equipped with filters for humidity (molecular sieves grade 5 and potassium permanganate) and organic compounds (carbon active) achieving a humidity of ~20 ppm.

2.3 Computational details

Structures of all neutral molecules, deprotonated ions and adduct anions were fully optimized by density functional theory (DFT) with ωB97xD functional and the basis set 6-311++G(d,p). Frequency calculations were performed at the same level of theory to obtain enthalpies and Gibbs free energies of deprotonation and adduct formation reactions in the gas phase. Gaussian 16 software was used for the calculations.[39]

3. Results and discussion

3.1 Reactant ions

Figure 1a compares the ion mobility spectra of the reactant ions generated in CD in the negative mode, with and without formic acid (FA) as a dopant gas, at 80 °C. The mass spectrum in the Figure 1b shows that the standard reactant ions in the negative mode are mainly O_2^- clusters with H_2O and CO_2, $O_2^-\cdot(CO_2)\cdot(H_2O)_{0,1}$ (m/z 76, 94). A weak peak with *m/z* of 60 ($N_2O_2^-/CO_3^-$) is also observed. Figure 1c shows that when the FA (headspace vapor) is used as dopant, it is deprotonated to produce $[FA\text{-}H]^-\cdot FA$ (or $HCOO^-\cdot FA$) cluster ions and it suppresses the standard reactant ions. Because of the high basicity of O_2^-, deprotonation of FA is an exothermic reaction with calculated reaction enthalpy (ΔH) of -36 kJ mol^{-1}. One of the practical advantages of the FA dopant, compared to $CHCl_3$ dopant, is lower sensitivity to the adjustment of the dopant flow rate. In the case of $CHCl_3$, at low dopant flow rates, both standard RIs and Cl^- are available. At increased $CHCl_3$ flow rates, the standard reactant ions are suppressed, but the dimer ions $(CHCl_3)\cdot Cl^-$ (or Cl_2^-) appear in the spectrum,[40,41] that may interfere with the analyte peaks. The ion mobility peak of $HCOO^-\cdot FA$ with the FA dopant appears at drift times close to the standard reactant ion peaks which reduces the interference. It should be mentioned that FA headspace flow rates below 5 mL min^{-1} were tried to avoid its dimerization ($HCOO^-\cdot FA$), however, with lower flow rates, there are still some peaks for the O_2^- and its clusters (Figure S2). Another advantage of the FA dopant is the basicity of formate anion, with a value between that of O_2^- and Cl^- anions. The

proton affinities of O_2^-, $HCOO^-$, Cl^-, and Br^- are 1474.2, 1438.2, 1394.9,[42] and 1353.7 kJ mol^{-1},[1,43] respectively, indicating that formate anion fills the large basicity gap between the two important reactant ions O_2^- and Cl^-. This provides more selectivity for the measurement of analytes within this basicity range.

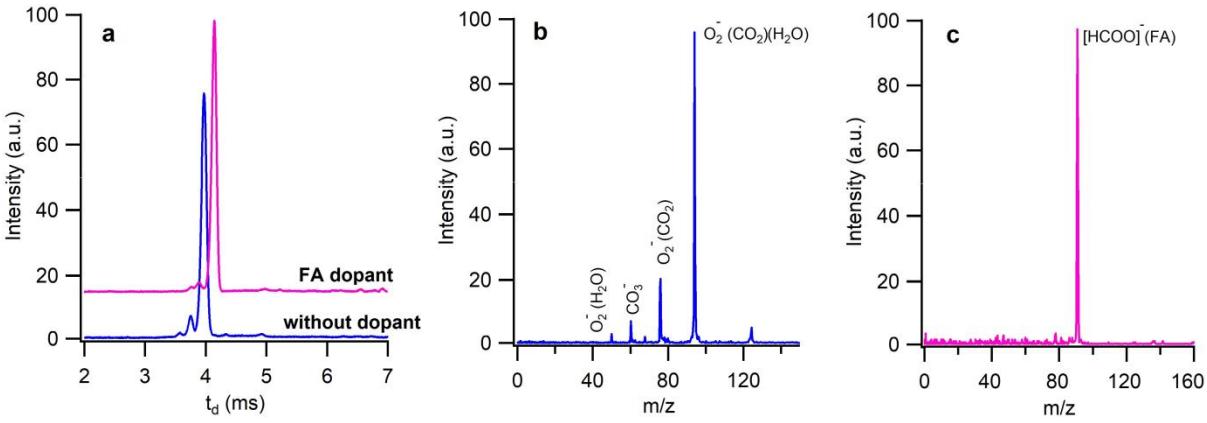

Figure 1. (a) Ion mobility spectra of the reactant ions in the negative mode with FA dopant and standard reactant ions. The mass spectra of (b) standard reactant ions and (c) reactant ions with FA dopant.

The main RI of FA is $HCOO^-{\cdot}FA$ with dissociation enthalpy of 115.2 kJ mol^{-1}. However, since the dissociation of this cluster (reaction 1) is a prerequisite for both ionization pathways, deprotonation (reaction 2) and $HCOO^-$ attachment (reaction 3), considering only the $HCOO^-$ reactions is adequate as means of comparing the thermodynamics of these parallel and competitive reactions.

$$HCOO^-{\cdot}FA \rightarrow HCOO^- + FA \quad (1)$$

$$HCOO^- + M \rightarrow [M\text{-}H]^- + FA \quad (2)$$

$$HCOO^- + M \rightarrow [M+HCOO]^- \quad (3)$$

Furthermore, a more realistic mechanism is the attachment of $HCOO^-{\cdot}FA$ to M to form an intermediate adduct ion. Then, the short-live intermediate adduct $[HCOO^-{\cdot}FA{\cdot}M]^{*-}$ undergoes collisional dissociation:[29]

$$HCOO^-{\cdot}FA + M \rightarrow [HCOO^-{\cdot}FA{\cdot}M]^{*-} \rightarrow [M\text{-}H]^- + 2FA \quad (4a)$$

$\rightarrow [M+HCOO]^- + FA$ (4b)

Hence, for the calculations of the thermodynamic data for the reactions, non-solvate form of the reactant ion, i.e. $HCOO^-$, was considered.

3.2 Plant hormones

Cytokines and auxins are two important classes of plant hormones, with completely different chemical structures.[44] However, both compounds exhibit strong acidity in the gas phase and thus are suitable to be studied in the negative polarity.[31,45,46] Figures 2a and 2b show the ion mobility spectra of BAP and IAA as examples of cytokines and auxins, respectively. The ion mobility spectrum of BAP shows a peak at 6.7 ms for standard ionization (without dopant), whereas in the presence of FA dopant, a peak at 7.2 ms appears. The signal intensity of BAP peak increased for ionization with FA dopant. The corresponding mass spectra (Figure 2b and 2c) show that standard ionization resulted in deprotonation and formation of $[M-H]^-$ ion, while ionization with FA dopant resulted in the formation of ions by formate attachment $[M+HCOO]^-$. The calculation data in the Table 1 show that although both standard and FA reactant ions can deprotonate BAP, deprotonation of BAP by O_2^- is thermodynamically more favoured than that by $HCOO^-$, by about 40 kJ mol^{-1}. Calculations show that the imidazole proton is the most acidic proton of BAP in the gas phase (Figure S3). Furthermore, $HCOO^-$ attachment to BAP (ΔG=-143.3 kJ mol^{-1}, Table 2) is more favoured than the parallel reaction of proton abstraction by $HCOO^-$. Hence, ionization in the presence of FA dopant leads to formation of the adduct anion $[BAP+HCOO]^-$. The optimized structures of the $[BAP+HCOO]^-$ adduct ions are shown Figure S4. BAP has two anion receptor groups, the imidazole and amine hydrogens, which simultaneously interact with the oxygen atoms of $HCOO^-$. This strong interaction leads to higher signal intensity of BAP with FA dopant and consequently, an increase in sensitivity materializes as a LOD decrease from 10 ng to 0.8 ng.

The ion mobility spectrum IAA (Figure 2d) in standard ionization exhibits three peaks between drift times 5.5 to 6.5 ms. The corresponding mass spectrum shows that ionization

by standard ions results in fragmentation, deprotonation, and O_2^- attachment (Figure 2e). The COOH group is the most acid site of IAA and is deprotonated by O_2^- with the calculated ΔH and ΔG of -43.0 and -54.0 kJ.mol^{-1}, respectively. The O_2^- attachment is also a thermodynamically favourable reaction with ΔG of -130.5 kJ mol^{-1}. In the mass spectrum we see a peak for the adduction $[IAA+O_2]^-$ and a more intense peak for deprotonated ion $[IAA-H]^-$. In the $[IAA+O_2]^-$, due to the exothermicity of the reaction, the proton is transferred to O_2^- and the product anion is in fact $[IAA-H]^-\cdot(HO_2)$, hence, after dissociation, an intense peak is detected for $[IAA-H]^-$.[31] In the case of FA dopant ionization, the deprotonation energy of IAA by the $HCOO^-$ ion is small (ΔG=-11.6 kJ mol^{-1}), while the interaction energy of adduct formation is relatively high (ΔG= -91.4 kJ mol^{-1}). Hence, the ion mobility spectrum of IAA shows only one peak for the $[IAA+HCOO]^-$ adduct ion (Figure 2f). Other auxins, IPA and IBA, are weaker acids than IAA. Both standard and FA dopant ionization result in the appearance of only one ion mobility peak, $[M+O_2]^-$ and $[M+HCOO]^-$, respectively (Figure S5). However, the FA dopant ionization provides enhanced sensitivity.

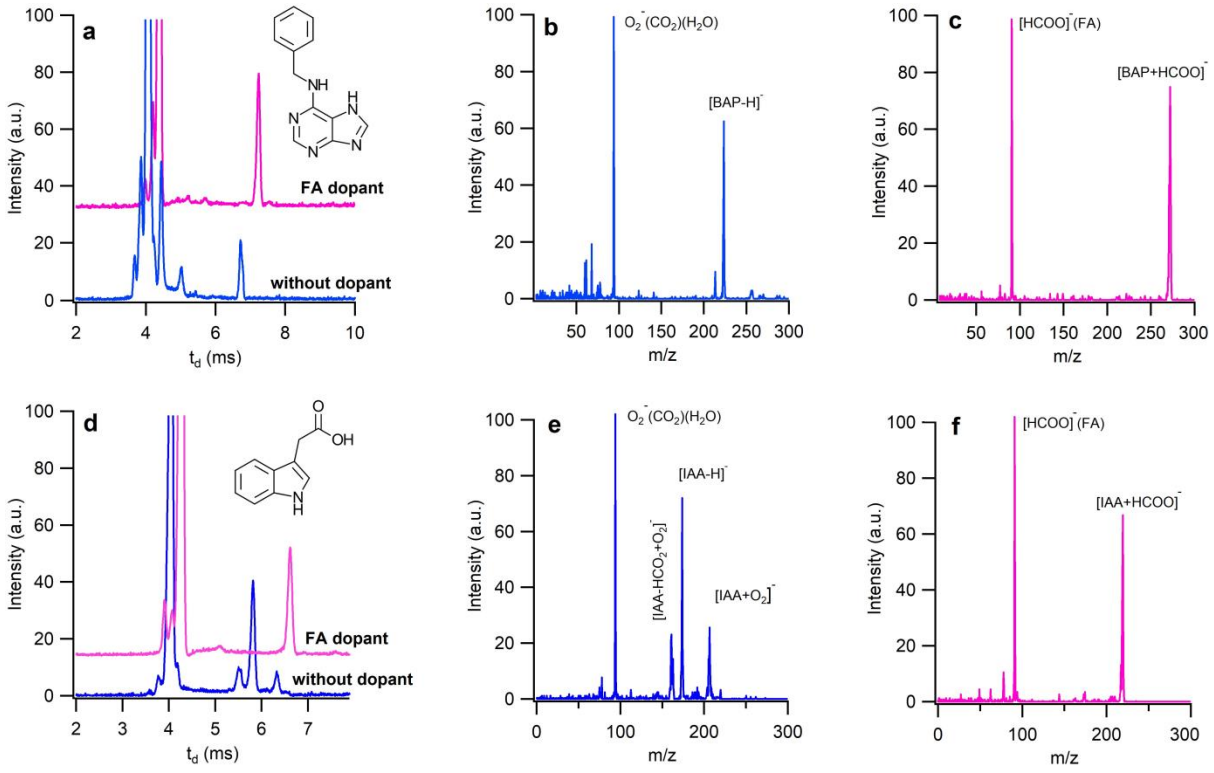

Figure 2. The ion mobility spectra of (a) BAP and (d) IAA with and without FA dopant. The mass spectra of (b) and (c) BAP and (e) and (f) IAA without and with FA dopant, respectively.

Table 1. The calculated ΔH and ΔG values for deprotonation of the studied compounds by O_2^- and $HCOO^-$ reactant ions at 298 K. The energies are in kJ mol^{-1}.

Deprotonation by O_2^-	ΔH	ΔG	Deprotonation by HCO_2^-	ΔH	ΔG
BAP + O_2^- → $[BAP-H]^-$ + HO_2	-93.4	-100.4	BAP + $HCOO^-$ → $[BAP-H]^-$ + HCO_2H	-57.4	-58
IAA + O_2^- → $[IAA-H]^-$ + HO_2	-43.0	-54.0	IAA + $HCOO^-$ → $[IAA-H]^-$ + HCO_2H	-7.0	-11.6
Asp + O_2^- → $[Asp-H]^-$ + HO_2	-78.5	-83.5	Asp + $HCOO^-$ → $[Asp-H]^-$ + HCO_2H	-42.5	-41.1
SA + O_2^- → $[SA-H]^-$ + HO_2	-97.2	-103.4	SA + $HCOO^-$ → $[SA-H]^-$ + HCO_2H	-61.2	-61.0
Nap + O_2^- → $[Nap-H]^-$ + HO_2	-58.8	-65.4	Nap + $HCOO^-$ → $[Nap-H]^-$ + HCO_2H	-22.8	-23.0
MCPA + O_2^- → $[MCPA-H]^-$ + HO_2	-76.3	-84.3	MCPA + $HCOO^-$ → $[MCPA-H]^-$ + HCO_2H	-40.3	-41.9
Kin + O_2^- → $[Kin-H]^-$ + HO_2	-88.9	-95.1	Kin + $HCOO^-$ → $[Kin-H]^-$ + HCO_2H	-52.9	-52.7
Adn + O_2^- → $[Adn-H]^-$ + HO_2	-53.0	-56.9	Adn + $HCOO^-$ → $[Adn-H]^-$ + HCO_2H	-17.0	-14.5
RDX + O_2^- → $[RDX-H]^-$ + HO_2	-28.6	-35.8	RDX + $HCOO^-$ → $[RDX-H]^-$ + HCO_2H	7.4	6.6
TNT + O_2^- → $[TNT-H]^-$ + HO_2	-123.4	-131.5	TNT + $HCOO^-$ → $[TNT-H]^-$ + HCO_2H	-87.4	-89.1

Table 2. The calculated ΔH and ΔG values for the formation of adduct anions of the studied compounds with formate $HCOO^-$ anion, $[M+HCOO]^-$, in the gas phase and at 298 K. For the adduct ions that undergo internal proton transfer to form $[M-H]^-(HCO_2H)$, the formation energies have been corrected for the proton transfer energies (numbers in parenthesis).

Formate attachment	ΔH (kJ mol^{-1})	ΔG (kJ mol^{-1})
BAP + HCO_2^- → $[BAP+HCOO]^-$	-184.4	-143.3
IAA + HCO_2^- → $[IAA+HCOO]^-$	-130.5 (-123.5)	-91.4 (-79.8)
Asp + HCO_2^- → $[Asp+HCOO]^-$	-146.9 (-104.4)	-107.8 (-66.7)
SA + HCO_2^- → $[SA+HCOO]^-$	-165.4 (-104.2)	-128.1 (-67.1)
Nap + HCO_2^- → $[Nap+HCOO]^-$	-126.8 (-104.0)	-82.4 (-59.4)
MCPA + HCO_2^- → $[MCPA+HCOO]^-$	-163.3 (-123.0)	-117.2 (-75.3)

Kin + HCO_2^- → $[Kin+HCOO]^-$	-202.0	-155.0
Adn + HCO_2^- → $[Adn+HCOO]^-$	-132.6	-83.9
RDX + HCO_2^- → $[RDX+HCOO]^-$	-198.9	-154.6
TNT + HCO_2^- → $[TNT+HCOO]^-$	-108.6 (-21.2)	-83.1 (6.0)

239

240

241 **3.3. Acidic drugs and pesticides**

242 The negative polarity of IMS is widely used for the detection of acidic drugs and pesticides or
243 substances containing electronegative groups.[47-49] Salicylic acid (SA), aspirin, and naproxen
244 were investigated in the negative polarity as typical examples of acidic drugs, and 2-methyl-
245 4-chlorophenoxyacetic acid (MCPA) as a typical pesticide. Figure 3a shows the ion mobility
246 spectra of SA in the negative polarity, as measured using standard and FA dopant
247 ionization. An ion mobility peak is observed at 5.1 ms under both ionization conditions,
248 however, ionization with FA dopant resulted in a lower intensity. Figure 3b and 3c shows that
249 SA is ionized via deprotonation and formation of $[SA-H]^-$ in the standard and FA dopant
250 ionization. According to Table 1, SA (along with TNT) is one of the strongest acids studied in
251 this work, hence, its deprotonation by both O_2^- and $HCOO^-$ is thermodynamically possible.
252 However, deprotonation by O_2^- is more favourable than that by $HCOO^-$ by about 40 kJ mol^{-1},
253 hence, FA dopant decreases the sensitivity of IMS for SA measurement.
254 Aspirin (acetylsalicylic acid) is a derivative of SA with lower acidity than SA, however, its
255 ionization is somewhat different from SA. Figure S6 shows the ion mobility and mass spectra
256 of aspirin in the negative polarity with standard ionization and with the addition of FA dopant.
257 In the standard ionization, the ion mobility spectrum of aspirin exhibits an intense peak at
258 4.3 ms, which was identified by the mass spectrometer as a fragment of aspirin with *m/z* of
259 92, produced due to ($COOH+COCOH_3$) loss (Figure S6b). This fragment has been
260 previously observed for aspirin.[50] The small peak at drift time of 4.9 ms is due to $COCOH_3$
261 loss and formation of $[SA-H]^-$ with *m/z* of 137. In the case of ionization with FA dopant, the
262 peak at 4.3 ms is suppressed, and only an intense peak at 4.9 ms is observed. The mass

spectrum in Figure S6c shows that the peak with *m/z* of 137 is either $[SA-H]^-$, or an adduct produced by the attachment of $HCOO^-$ to the fragment with *m/z* of 92. The LOD for aspirin was equal for standard and FA dopant ionization, achieving a value of 0.5 ng. However, with the FA dopant, both fragment suppression and drift time shift were observed, which can be important in the case of mixture sample measurements, where peak overlap could be an issue.

Figure 3d presents the ion mobility spectra of naproxen (2-(6-Methoxynaphthalen-2-yl) propanoic acid) obtained using the standard and FA dopant ionization methods. For standard ionization, two peaks at 7.18 and 7.42 ms were observed. The mass spectrum in Figure 3e shows that these peaks represent deprotonated naproxen ion and its O_2^- adduct ion, respectively. According to Table 1, naproxen has a moderate gas phase acidity (similar to auxins), hence, it has a similar ionization mechanism. However, due to the stronger acidity of naproxen (by about 15 kJ mol^{-1} compared to IAA), more deprotonation was observed in comparison to IAA. In the case of FA dopant ionization, an ion mobility peak at 7.65 was observed for naproxen, identified as $[Nap+HCOO]^-$ adduct ion (Figure 3f). A weak signal for $[Nap-H]^-$ was also detected in the mass spectrum (Figure 3f), which was not observable in IMS spectrum (Figure 3d), most likely due to its low intensity or merging into the $[Nap+HCOO]^-$ peak. FA dopant ionization of naproxen resulted in a sensitivity improvement compared to standard ionization, with LODs decreasing in half, from 10 ng to 5 ng.

The ion mobility spectra of MCPA recorded using the standard and FA ionization methods are compared in Figure 3g. Standard ionization resulted in the appearance of a strong IMS peak at 6.32 ms and two weaker peaks at 5.62 and 6.58 ms. The most intense peak was identified by mass spectrometry as $[MCPA-H]^-$. MCPA is a stronger acid than naproxen by about 20 kJ mol^{-1} (Table 1), hence, a more intense peak was observed for its deprotonated ions. The weak peak at the lower drift times is an adduct ion of the fragment (MCPA-CH_2CO_2) with O_2^- and the other peak at 6.58 ms is the adduct ion of MCPA with O_2^- (Figure 3h). FA dopant ionization resulted in the appearance of a new peak at 6.83 ms, identified as $[MCPA+HCOO]^-$adduct ion (Figure 3i), while the deprotonated and fragmented ions

generated by the standard ionization method were not detected. The optimized structures for the most stable isomers of the $[M+HCOO]^-$ adduct ion of aspirin, SA, Naproxen and MCPA are shown in Figure S7. The calculations showed a strong interaction between MCPA and $HCOO^-$, with ΔH of adduct formation of -163.3 kJ mol^{-1}. Hence, the formation of the $[MCPA+HCOO]^-$ adduct ion is thermodynamically more favoured than the formation of $[Nap+HCOO]^-$ adduct ion, by about 40 $kJmol^{-1}$. The formation of this stable adduct ion of MCPA led to a considerable sensitivity enhancement so that the FA dopant has improved the LOD of MCPA from 12 ng to 2 ng.

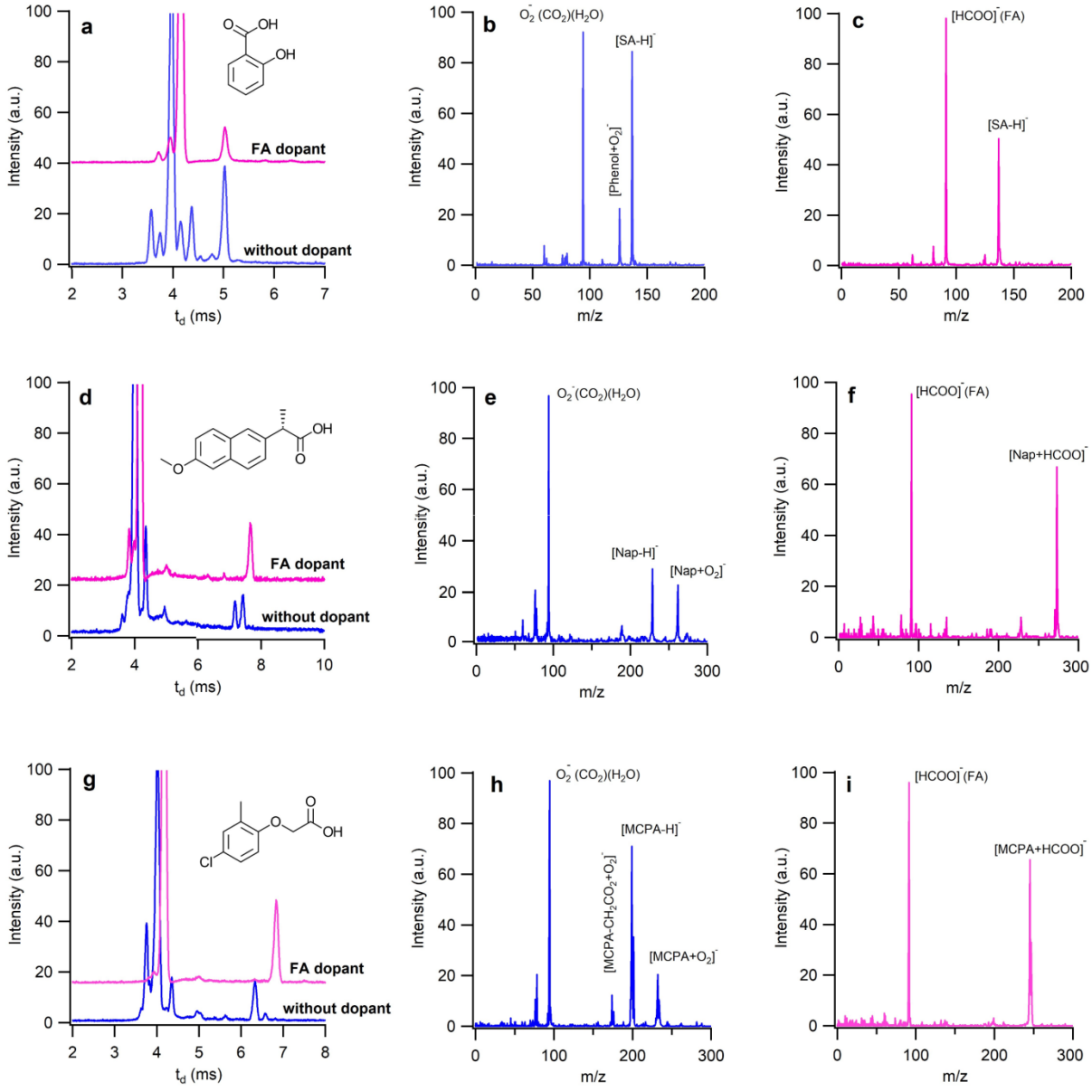

Figure 3. Comparison of ion mobility spectra of (a) salicylic acid (SA), (d) naproxen, and (g) MCPA, alongside with mass spectra - (b,c) SA, (e,f) naproxen and (h,i) MCPA, with (pink) and without (blue) FA dopant.

3.4 Explosives

Detection of explosives is one of the traditional applications of IMS in the negative polarity.[51-53] Figure 4a shows the ion mobility spectra of RDX in the negative polarity, ionized using both standard and FA dopant ionization. In the case of standard ionization, an ion mobility peak was observed at 6.24 ms accompanied by fragment peaks at lower drift times. The corresponding mass spectrum in Figure 4b shows that the peak at 6.24ms is the adduct anion $[RDX+NO_2]^-$ and the fragment peaks are mainly due to NO_2 cleavage from RDX, which agrees with previous studies.[4,54-56] A weak peak was also observed for the deprotonated RDX, $[RDX-H]^-$. The FA dopant ionization suppresses all the fragment peaks and only an intense peak at 6.28 ms is observed in the spectrum (Figure 4a). The mass spectrum in Figure 4c shows that this single peak is the adduct anion $[RDX+HCOO]^-$. This adduct ion has been previously observed for RDX in an electrospray ionization source.[57] The calculated ΔH and ΔG values for deprotonation reactions in Table 1 shows that deprotonation of RDX by the standard RI ($O_2^-\cdot(CO_2)_1(H_2O)_{0,1}$) is thermodynamically possible (-28.6 and -35.8 kJ mol^{-1}, respectively), while deprotonation by $HCOO^-$ is not favourable (7.4 and 6.6 kJ mol^{-1}, respectively). Furthermore, the G4MP2-calculated electron affinities (EA) of O_2 and HCO_2 (0.42 and 3.52 eV, respectively) indicate higher ability of O_2^- to ionize the analyte via electron transfer reaction, as compared to formate anion $HCOO^-$. Fragmentation of ions occurs upon charge transfer and proton (hydride) abstraction reactions,[14,58] hence, the fragmentation of RDX under standard ionization takes place because O_2^- preferentially ionizes RDX via charge transfer and deprotonation reactions. The thermodynamic properties of $HCOO^-$ make it a reactant ion for soft ionization of RDX via adduct ion formation reaction. The optimized structure of the adduct anion $[RDX+HCOO]^-$ in Figure 5 shows that the RDX

structure is converted from its planar to a bowl-shape geometry, for a more suitable interaction with $HCOO^-$ via its three H atoms. This geometry leads to strong interaction between $HCOO^-$ and RDX, with calculated ΔH and ΔG of -198.9 and -154.6 $kJmol^{-1}$, respectively (Table 2). The ionization of RDX using the FA dopant resulted in sensitivity improvement by more than one order of magnitude and the limit of detection (LOD) decreased from 5 ng to 0.2 ng. The effect of FA dopant ionization on RDX is similar to its effect of IAA (Figure 2a) in both cases the FA dopant suppresses fragmentation, leading to a simple ion mobility spectrum with only one intense peak. However, in the case of IAA, the sensitivity improvement is not as much as it was for RDX. The LOD of IAA for standard ionization was 12 ng and in the case of FA it had improved to 7 ng. This is most likely due to the weaker interaction of IAA and $HCOO^-$ (ΔH=-130.5 kJ mol^{-1}), compared to RDX and $HCOO^-$ (ΔH=-198.9 kJ mol^{-1}).

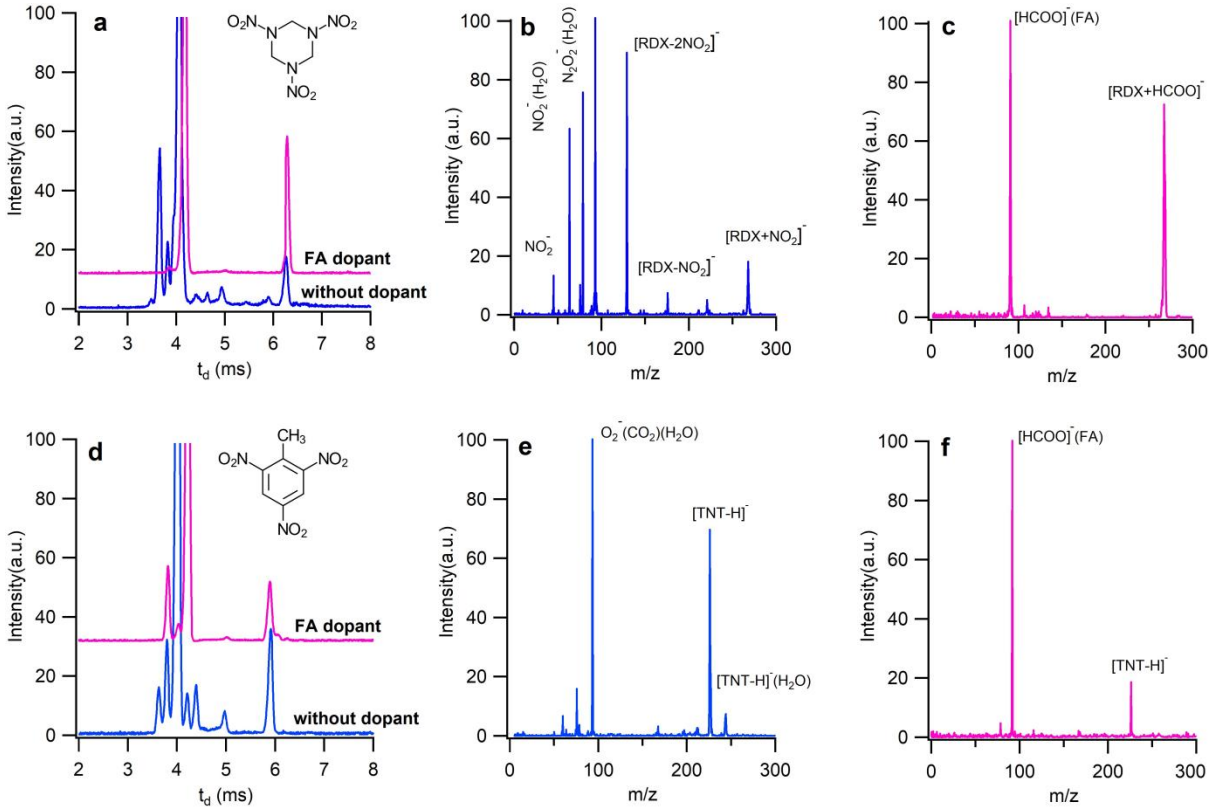

Figure 4. Comparison of the ion mobility spectra of (a) RDX and (d) TNT, alongside mass spectra of (b, c) RDX and (e,f) TNT without (blue) and with (pink) FA dopant.

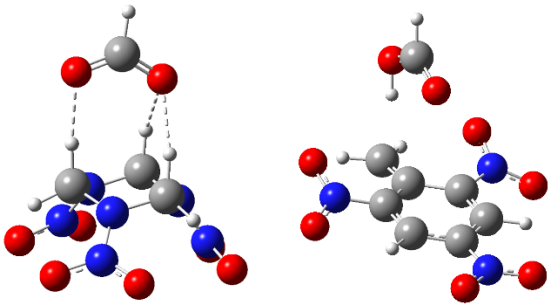

Figure 5. Optimized structures of adduct anions of $[RDX+HCO_2]^-$ and $[TNT+HCO_2]^-$. Because of the high acidity of TNT, $[TNT+HCO_2]^-$ converts to [TNT-H](FA) via intermolecular proton transfer.

Ion mobility spectra for standard ionization and FA dopant ionization of TNT (Figure d) exhibit only one peak at 5.9 ms. The corresponding mass spectra in Figures 4e and 4f reveal that this peak corresponds to deprotonated TNT ion, $[TNT-H]^-$. The calculated values of ΔH and ΔG in Table 1 show that deprotonation of TNT with both O_2^- (ΔG=-131.5 kJ mol^{-1}) and $HCOO^-$ (ΔG=-89.1 kJ mol^{-1}) is thermodynamically possible, however, deprotonation by O_2^- is more favoured, which provides a reason why the ionization using FA dopant is less efficient. Because of high gas phase acidity of TNT (ΔH_{acid}=1350.8 kJ mol^{-1}, comparable with gas phase acidity of HBr), it does not form an adduct anion with $HCOO^-$. The optimized structure of $[TNT+HCOO]^-$ in Figure 5 shows that the proton of CH_3 group of TNT is transferred to $HCOO^-$ to form $[TNT-H]^-\cdot$(FA) complex. TNT and SA are typical examples, for which the ionization using FA dopant has a destructive effect on their signal intensity, or sensitivity. The results for TNT show that, for compounds with very strong gas phase acidity without anion receptor groups, measurements with standard reactant ions such as O_2^- lead to more promising results.

3.5 Effect of temperature

All the measurements presented so far were performed at a drift temperature of 80 °C. However, to investigate effect of temperature on the ionization mechanism with FA dopant, the measurements were repeated at 120°C for selected compounds with a range of acidities (TNT > BAP >kinetin >adenine). The ionization mechanism for TNT at 80 and 120 °C was the same and only deprotonated ions $[TNT-H]^-$ were observed at both temperatures. This is because of the high acidity of TNT (the strongest acid in Table 1) and corresponding lowest tendency for adduct formation with $HCOO^-$. Figure 6 presents the mass spectra of BAP, kinetin and adenine ionized in the presence of the FA dopant at the two temperatures of 80 and 120 °C. For BAP, kinetin, and adenine, only the adduct ions $[M+HCOO]^-$ were observed at 80 °C. However, at the elevated temperature of 120 °C, the ionization pathways for these compounds changed. At 120 °C, the deprotonated ions of BAP and kinetin appeared. The formation of deprotonated ions is due to dissociation of the $[M+HCOO]^-$ adducts to $[M-H]^-$ and FA, taking place at the higher temperature. The stronger relative intensity of $[BAP-H]^-$ peak compared to $[Kin-H]^-$ peak is because of the higher acidity of BAP in comparison to kinetin (Table 1) and the stronger kinetin/$HCOO^-$ interaction in the adduct anion (Table 2). In the case of adenine (weak acid), only the adduct ion $[Adn+HCOO]^-$ was observed at both temperatures. Although we expect a decrease in the intensity of the $[Adn+HCOO]^-$ peak at 120 °C due to its dissociation to adenine and $HCOO^-$, the intensity is approximately constant at both temperatures. This is because of the shorter drift time of this adduct ion at the higher temperature (Figure S8), which decreases the ion loss in the drift tube and compensates for the adduct dissociation.

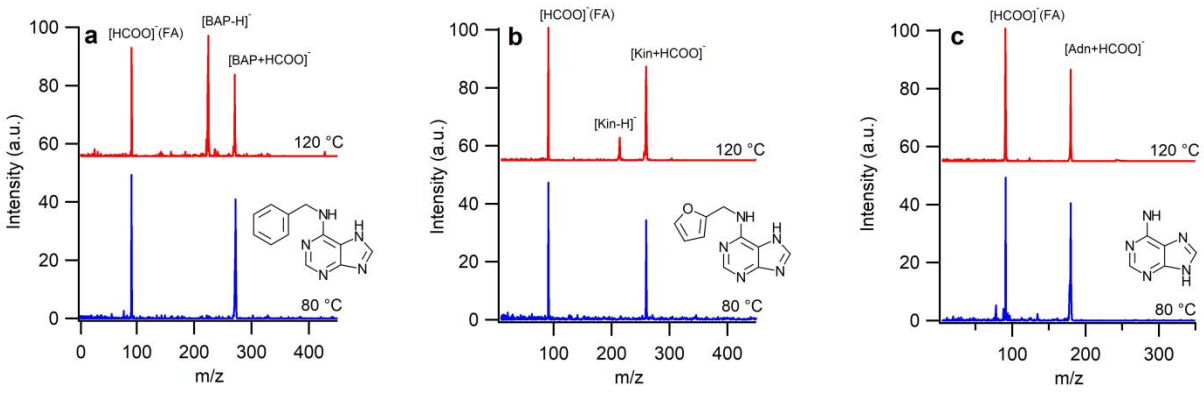

Figure 6. Mass spectra of (a) BAP, (b) kinetin, and (c) adenine recorded with FA dopant at the temperatures of 80 (blue) and 120 (red) °C.

4. Conclusion

Formic acid (FA) was introduced as a dopant for ionization in the negative polarity of CD-IMS. A systematic investigation was performed to assess the effect of this dopant on the detection of different classes of compounds with COOH, OH, CH, and NH functional groups as deprotonation sites. It was found that FA can ionize the compounds via two competitive reactions, deprotonation and adduct formation with $HCOO^-$. The interpretation of the experimental results was supported by DFT calculations. It was found that the ionization mechanism and consequently the measurement sensitivity depends on the gas phase acidities of the analytes and their interaction energy with the $HCOO^-$ ion. For strong gas phase acids, such as TNT and SA, the sole ionization mechanism was deprotonation and FA dopant decreased the sensitivity as $HCOO^-$ is a weaker base than the O_2^- reactant ion. In contrast, in the case of weak acids (IAA, RDX,..), ionization with the FA dopant led to both sensitivity enhancement and simplification of the ion mobility spectrum, due to ionization via $HCOO^-$ attachment. For the compounds with moderate gas phase acidities, the effect of FA dopant depended on the reaction enthalpy of adduct formation with $HCOO^-$. As the cytokine plant hormones exhibited high affinity toward $HCOO^-$ (strong interaction), measurements in the presence of FA improved their LODs. For auxin plant hormones and naproxen, with weaker interaction to $HCOO^-$ relative to cytokines, a considerable improvement in sensitivity was not observed. For all the studied compounds (except TNT and SA) an IMS peak shift to higher drift times were observed, which can be considered as one of the advantages of FA dopant ionization. Furthermore, adjustment of the FA flow rate in order to establish a stable reactant ion current was simple, which is very useful in experimental works. Finally, the effect of drift temperature on the ionization mechanism was considered and it was found that

at higher temperatures, the $[M+HCOO]^-$ adduct dissociation occurs and the nature of the product ions depend on the acidity of the compound.

Supporting Information

Schematic representation of the experimental setup (Figure S1);The mass spectrum of formic acid FA in the negative mode (Figure S2);The optimized structures of different isomers of $[BAP-H]^-$ (Figure S3);The optimized structures of different isomers of $[BAP+HCOO]^-$ (Figure S4);Comparison of the ion mobility and mass spectra IPA and IBA with and without FA dopant (Figure S5);Comparison of the ion mobility and mass spectra of aspirin with and without FA dopant (Figure S6);The optimized structures of the most stable isomers of adduct anions (Figure S7);Comparison of the ion mobility spectra of Adenine with FA dopant at two drift temperatures of 80 and 120°C (Figure S8).

Author Information

Corresponding Authors

VahidehIlbeigi, Department of Experimental Physics, Faculty of Mathematics, Physics and Informatics, Comenius University in Bratislava, Mlynská dolina F2, 84248 Bratislava, Slovakia; orcid.org/0000-0001-9112-8381.

ŠtefanMatejčík, Department of Experimental Physics, Faculty of Mathematics, Physics and Informatics, Comenius University in Bratislava, Mlynská dolina F2, 84248 Bratislava, Slovakia; orcid.org/0000-0001-7238-5964.

Authors

Younes Valadbeigi, Department of Chemistry, Faculty of Science, Imam Khomeini International University, Qazvin, Iran; orcid.org/0000-0002-4189-2987.

Ladislav Moravsky, Department of Experimental Physics, Faculty of Mathematics, Physics and Informatics, Comenius University in Bratislava, Mlynská dolina F2, 84248 Bratislava, Slovakia orcid.org/0000-0003-2579-5607.

Notes

The authors declare no competing financial interest.

Acknowledgments

The research presented in this paper received funding from the European Union's Horizon 2020 research and innovation programme under the Marie Sklodowska-Curie grant agreement No 101031538 and was partially supported by Slovak Research and Development Agency under project Nr. APVV-19-0386.

References

(1) Eiceman, G. A.; Karpas, Z.; Hill, H. H. Ion Mobility Spectrometry (3rd ed.). CRC Press, Taylor & Francis Group, Boca Raton, FL,2014.

(2) D'Atri, V.; Causon, T.; Hernandez-Alba, O.; Mutabazi, A.; Veuthey, J. L.; Cianferani, S.; Guillarme, D. Adding a New Separation Dimension to MS and LC-MS: What Is the Utility of Ion Mobility Spectrometry?.*J. Sep. Sci.***2018,***41*,20-67.

(3) Armenta, S.; Alcala, M.; Blanco, M. A Review of Recent, Unconventional Applications of Ion Mobility Spectrometry (IMS). *Anal. Chim. Acta.***2011,***703*, 114-123.

(4) Ewing, R.G.; Atkinson, D.A.; Eiceman, G.A.; Ewing, G.J. A Critical Review of Ion Mobility Spectrometry for the Detection of Explosives and Explosive Related Compounds. *Talanta*, **2001,***54*, 515-529.

(5) Tabrizchi, M.; ILbeigi V. Detection of Explosives by Positive Corona Discharge Ion Mobility Spectrometry. *J. Hazard. Mater*. **2010,***176*, 692-696.

(6) Mäkinen, M. A.; Anttalainen, O. A.; Sillanpää, Mika E. T. Ion Mobility Spectrometry and Its Applications in Detection of Chemical Warfare Agents. *Anal. Chem*. **2010,***82*, 9594–9600.

(7) Fytche, L. M.; Hupé, M.; Kovar, J. B.; Pilon, P. Ion Mobility Spectrometry of Drugs of Abuse in Customs Scenarios: Concentration and Temperature Study. *J. Forensic Sci*. **1992,***37*, 1550-1566.

(8) Denia, A.; Esteve-Turrillas, F. A.; Armenta, S. Analysis of Drugs Including Illicit and New Psychoactive Substances in Oral Fluids by Gas Chromatography-Drift Tube Ion Mobility Spectrometry. *Talanta,***2022,***238*, 122966.

(9) Brinke, E. te.; Arrizabalaga-Larrañaga, A.; Blokland, M. H. Insights of Ion Mobility Spectrometry and Its Application on Food Safety and Authenticity: A Review. *Anal. Chim. Acta.***2022,***1222*, 340039.

(10) Vautz, W.; Nolte, J.; Bufe, A.; Baumbach, J. I.; Peters, M. Analyses of Mouse Breath with Ion Mobility Spectrometry: AFeasibilityStudy. *J. Appl. Physiol.***2010,***108*, 697-704.

(11) Bruderer, T.; Gaisl, T.; Gaugg, M. T.; Nowak, N.; Streckenbach, B.; Müller, S.; Moeller, A.; Kohler, M.; Zenobi, R. On-Line Analysis of Exhaled Breath. *Chem. Rev.***2019,***119*, 10803–10828.

(12) Dzidic, I.; Carroll, D. I.; Stillwell, R. N.; Horning, E. C. Comparison of Positive Ions Formed in Nickel-63 and Corona Discharge Ion Sources Using Nitrogen, Argon, Isobutane, Ammonia and Nitric Oxide as Reagents in Atmospheric Pressure Ionization Mass Spectrometry. *Anal. Chem.***1976**, *48*, 1763–1768.

(13) Sunner, J.; Nicol, G.; Kebarle, P. Factors Determining Relative Sensitivity of Analytes in Positive Mode Atmospheric Pressure Ionization Mass Spectrometry. *Anal. Chem.***1988,***60*, 1300–1307.

(14) Valadbeigi, Y.; Causon, T. Significance of Competitive Reactions in an Atmospheric Pressure Chemical Ionization Ion Source: Effect of Solvent. *J. Am. Soc. Mass Spectrom.***2022**, *33*, 961–973.

(15) Budzyńska, E.; Wolańska, I.; Puton, J. Negative-Mode Ion Mobility Spectrometry—Comparison of Ion–Molecule Reactions and Electron Capture Processes. *Anal. Bioanal. Chem.***2022**, *414*, 3719-3728.

(16) Sabo, M.; Okuyama, Y.; Kucera, M.; Matejcik, S. Transport and Stability of Negative Ions Generated by Negative Corona Discharge in Air Studied Using Ion Mobility-oaTOF Spectrometry. *Int.J. Mass Spectrom.***2013,***334*, 19-26.

(17) Allers, M.; Kirk, A. Timke, T.; B.; Erdogdu, D.; Wissdorf, W.; Benter, T.; Zimmermann, S. Negative Reactant Ion Formation in High Kinetic Energy Ion Mobility Spectrometry (HiKE-IMS). *J. Am. Soc. Mass Spectrom.***2020,***31*, 1861–1874.

(18) Valadbeigi, Y.; Ilbeigi, V.; Michalczuk, B.; Sabo, M.; Matejcik, S. Effect of Basicity and Structure on the Hydration of Protonated Molecules, Proton-Bound Dimer and Cluster Formation: An Ion Mobility-Time of Flight Mass Spectrometry and Theoretical Study. *J. Am. Soc. Mass Spectrom.***2019,***30*, 1242–1253.

(19) Puton, J.; Nousiainen, M.; Sillanpää, M. Ion Mobility Spectrometers with Doped Gases. *Talanta,***2008,***76*, 978-987.

(20) Waraksa, E.; Perycz , U.; Namieśnik, J.; Sillanpää, M.; Dymerski,T.; Wójtowicz, M.; Puton, J. Dopants and Gas Modifiers in Ion Mobility Spectrometry. *Trend Anal. Chem.***2016**, *82*, 237-249.

(21) Fernández-Maestre, R.; Wu, C.; Hill, H. H. Buffer Gas Modifiers Effect Resolution in Ion Mobility Spectrometry Through Selective Ion-Molecule Clustering Reactions. *Rapid Commun. Mass Spectrom.***2012,***26*, 2211–2223.

(22) Valadbeigi, Y.; Bayat, S.; Ilbeigi, V. A Novel Application of Dopants in Ion Mobility Spectrometry: Suppression of Fragment Ions of Citric Acid*. Anal. Chem.***2020,***92*, 7924–7931.

(23) Liu, H.; Xia, L.; Shen, C.; Huang, C.; Chu, Y. Dopant for Detection of Methamphetamine in the Presence of Nicotine with Ion Mobility Spectrometry. *Anal. Bioanal. Chem.***2021,***413*, 4237-4246.

(24) Li, M.; Huang, W.; Chen, H.; Jiang, D.; Wang, W.; Xiao, Y.; Chen, C.; Li, H. Dopant Assisted Photoionization Ion Mobility Spectrometry for On-Site Specific and Sensitive Determination of Atmospheric Ammonia. *Sens. Actuators B Chem.***2021,***330*, 129365.

(25) Brendel, R.; Rohn, S.; Weller, P. Nitrogen Monoxide as Dopant for Enhanced Selectivity of Isomeric Monoterpenes in Drift Tube Ion Mobility Spectrometry with 3H Ionization. *Anal. Bioanal. Chem.***2021,***413*, 3551-3560.

(26) Meyer, N. A.; Root, K.; Zenobi, R.; Vidal-de-Miguel, G. Gas-Phase Dopant-Induced Conformational Changes Monitored with Transversal Modulation Ion Mobility Spectrometry. *Anal. Chem.***2016**, *88*, 2033–2040.

(27) Dwivedi, P.; Wu, C.; Matz, L. M.; Clowers, B. H.; Siems, W. F.; Hill, H. H. Gas Phase Chiral Separations By Ion Mobility Spectrometry. *Anal Chem.* **2006**, *78*, 8200–8206.

(28) Saraji, M.; Bidgoli, A. A. H.; Khayamian, T.; Moradmand, A. Combination of Corona Discharge Ion Mobility Spectrometry with a Novel Reagent Gas and Two Immiscible Organic Solvent Liquid–Liquid–Liquid Microextraction for Analysis of Clomipramine in Biological Samples. *J. Chromatogr. A*, **2011,***1218*, 8600-8607.

(29) Valadbeigi, Y.; Ilbeigi, V.; Michalczuk, B.; Sabo, M.; Matejcik, S. Study of Atmospheric Pressure Chemical Ionization Mechanism in Corona Discharge Ion Source with and without NH_3 Dopant by Ion Mobility Spectrometry Combined with Mass Spectrometry: A Theoretical and Experimental Study. *J. Phys. Chem. A*. **2019,***123*, 313–322.

(30) Gaik, U.; Sillanpää, M.; Witkiewicz, Z.; Puton, J. Nitrogen Oxides as Dopants for the Detection of Aromatic Compounds with Ion Mobility Spectrometry. *Anal. Bioanal. Chem.***2017,***409*, 3223-3231.

(31) Ilbeigi, V.; Valadbeigi, Y.; Moravsky, L.; Matejcik, S. Effect of Ion Source Polarity and Dopants on the Detection of Auxin Plant Hormones by Ion Mobility-Mass Spectrometry. *Anal. Bioanal. Chem.* **2022,***414*, 6259-6269.

(32) Valadbeigi, Y.; Azizmohammadi, S.; Ilbeigi, V. Small Host–Guest Systems in the Gas Phase: Tartaric Acid as a Host for both Anionic and Cationic Guests in the Atmospheric Pressure Chemical Ionization Source of Ion Mobility Spectrometry. *J. Phys. Chem. A*, **2020**, *124*, 3386–3397.

(33) Hauck, B. C.; Harden, C. S.; McHugh, V. M. Isoflurane as An Accurate Negative Mode Calibrant for Ion Mobility Spectrometry. *Anal. Chem.***2021**, *93*, 16142–16148.

(34) Gunzer, F.; Zimmermann, S. Investigation of Ion Cluster Formation in a Pulsed Ion Mobility Spectrometer Operating in the Negative Mode. *Sens. Actuators B Chem.***2014**, *204*, 467-473.

(35) González-Méndez, R.; Watts, P.; Howse, D. C.; Procino, I.; McIntyre, H.; Mayhew, C. A. Ion Mobility Studies on the Negative Ion-Molecule Chemistry of Isoflurane and Enflurane. *J. Am. Soc. Mass Spectrom.***2017**, *28*, 939–946.

(36) Eiceman, G. A.; Shoff, D. B.; Harden, C. S.; Snyder, A. P.; Martinez, P. M.; Fleischer, M. E.; Watkins, M. L. Ion Mobility Spectrometry of Halothane, Enflurane, and Isoflurane Anesthetics in Air and Respired Gases. *Anal. Chem.***1989**, *61*, 1093–1099.

(37) Li, H.; Bendiak, B.; Siems, W. F.; Gang, D. R.; Hill, H. H. Ion Mobility Mass Spectrometry Analysis of Isomeric Disaccharide Precursor, Product and Cluster Ions. *Rapid Commun. Mass Spectrom.***2013,** *27*, 2699-2709.

(38) Sabo, M.; Matejcik, S. Corona Discharge Ion Mobility Spectrometry with Orthogonal Acceleration Time of Flight Mass Spectrometry for Monitoring of Volatile Organic Compounds. *Anal. Chem.***2012,** *84*, 5327–5334.

(39) Frisch, M. J.; Trucks, G. W.; Schlegel, H. B.; Scuseria, G. E.; Robb, M. A.; Cheeseman, J. R.; Scalmani, G.; Barone, V.; Petersson, G. A.; Nakatsuji, H.; Li, X.; Caricato, M.; Marenich, A. V.; Bloino, J.; Janesko, B. G.; Gomperts, R.; Mennucci, B.; Hratchian, H. P.; Ortiz, J. V.; Izmaylov, A. F.; Sonnenberg, J. L.; Williams-Young, D.; Ding, F.; Lipparini, F.; Egidi, F.; Goings, J.; Peng, B.; Petrone, A.; Henderson, T.; Ranasinghe, D.; Zakrzewski, V. G.; Gao, J.; Rega, N.; Zheng, G.; Liang, W.; Hada, M.; Ehara, M.; Toyota, K.; Fukuda, R.; Hasegawa, J.; Ishida, M.; Nakajima, T.; Honda, Y.; Kitao, O.; Nakai, H.; Vreven, T.; Throssell, K.; Montgomery, J. A., Jr.; Peralta, J. E.; Ogliaro, F.; Bearpark, M. J.; Heyd, J. J.; Brothers, E. N.; Kudin, K. N.; Staroverov, V. N.; Keith, T. A.; Kobayashi, R.; Normand, J.; Raghavachari, K.; Rendell, A. P.; Burant, J. C.; Iyengar, S. S.; Tomasi, J.; Cossi, M.; Millam, J. M.; Klene, M.; Adamo, C.; Cammi, R.; Ochterski, J. W.; Martin, R. L.; Morokuma, K.; Farkas, O.; Foresman, J. B.; Fox, D. J. Gaussian 16, Revision C.01; Gaussian, Inc.: Wallingford CT, 2016.

(40) Valadbeigi, Y.; Ilbeigi, V.; Vahidi, M.; Michalczuk, B.; Matejcik, S.; Tabrizchi, M. Online Detection and Measurement of Elemental Mercury Vapor by Ion Mobility Spectrometry with Chloroform Dopant. *J. Chromatogr. A,* **2020,***1634*, 461676.

(41) Ewing, R. G.; Atkinson, D. A.; Benson, M. T. Atmospheric Pressure Ionization of Chlorinated Ethanes in Ion Mobility Spectrometry and Mass Spectrometry. *Int. J. Ion Mobil. Spectrom.***2015,***18*, 51-58.

(42) Martin, J. D. D.; Hepburn, J. W. Determination of Bond Dissociation Energies by Threshold Ion-Pair Production Spectroscopy: An Improved D-0(HCl). *J. Chem. Phys.***1998,***109*, 8139-8142.

(43) Blondel, C.; Cacciani, P.; Delsart, C.; Trainham, R. High Resolution Determination of the Electron Affinity of Fluorine and Bromine Using Crossed Ion and Laser Beams. *Phys. Rev. A,***1989,***40*, 3698.

(44) Waadt, R.; Seller, C. A.; Hsu, P. K.; Takahashi, Y.; Munemasa, S.; Schroeder, J. I. Plant Hormone Regulation of Abiotic Stress Responses. *Nat. Rev. Mol. Cell Biol.***2022,***23*, 680-694.

(45) Lu, Q.; Zhang, L.; Chen, T.; Lu, M.; Ping, T.; Chen, G. Identification and Quantitation of Auxins in Plants by Liquid Chromatography/Electrospray Ionization Ion Trap Mass Spectrometry. *Rapid Commun. Mass Spectrom.***2008,***22*, 2565-2572.

(46) Hocart, C. H.; Wang, J.; Letham, D. S. Derivatives of Cytokinins for Negative Ion Mass Spectrometry. *J. Chromatogr. A,***1998,***811*, 246-249.

(47) Baert, B.; Vansteelandt, S.; De Spiegeleer, B. Ion Mobility Spectrometry as a High-Throughput Technique for in vitro Transdermal Franz Diffusion Cell Experiments of Ibuprofen. *J. Pharm. Biomed. Anal.***2011,***55*, 472-478.

(48) Valadbeigi, Y.; Ilbeigi, V.; Afgar, A.; Soleimani, M. Comparison of the Positive and Negative Modes of Corona Discharge Ion Source for Direct Determination of Aspirin in Urine by Ion Mobility Spectrometry. *Int. J. Mass Spectrom.***2021,***470*, 116699.

(49) Gallart-Mateu, D.; Armenta, S.; de la Guardia, M. Indoor and Outdoor Determination of Pesticides in Air by Ion Mobility Spectrometry. *Talanta,***2016,***161*, 632-639.

(50) https://webbook.nist.gov/cgi/cbook.cgi?ID=C50782&Mask=200#Mass-Spec

(51) Eiceman, G.A.; Preston, D.; Tiano, G.; Rodriguez, J.; Parmeter, J. E. Quantitative Calibration of Vapor Levels of TNT, RDX, and PETN Using a Diffusion Generator with Gravimetry and Ion Mobility Spectrometry. *Talanta,***1997,***45*, 57-74.

(52) Shahraki, H.; Tabrizchi, M.; Farrokhpor, H. Detection of Explosives Using Negative Ion Mobility Spectrometry in Air Based on Dopant-Assisted Thermal Ionization. *J. Hazard. Mater.***2018,***357*, 1-9.

(53) Sabo, M.; Malaskova, M.; Matejcik, S. Laser Desorption with Corona Discharge Ion Mobility Spectrometry for Direct Surface Detection of Explosives. *Analyst,***2014,***139*, 5112-5117.

(54) Khayamian, T.; Tabrizchi, M.; Jafari, M. T. Analysis of 2,4,6-Trinitrotoluene, Pentaerythritol Tetranitrate and Cyclo-1,3,5-Trimethylene-2,4,6-Trinitramine Using Negative Corona Discharge Ion Mobility Spectrometry. *Talanta,***2003,***59*, 327-333.

(55) Lichvanova, Z.; Sabo, M.; Matejcik, S. The Study of Thermal Decomposition of RDX by Corona Discharge-Ion Mobility Spectrometry-Mass Spectrometry. *Int. J. Ion Mobili. Spectrom.***2015,***18*, 59-66.

(56) Florián, J.; Gao, L.; Zhukhovskyy, V.; Macmillan, D. K.; Chiarelli, M. P. Nitramine Anion Fragmentation: A Mass Spectrometric and Ab Initio Study. *J. Am. Soc. Mass Spectrom.***2007,***18*, 835-841.

(57) Park, S.; Lee, J.; Cho, S. G.; Goh, E. M.; Lee, S.; Koh, S. S.; Kim, J.; Mass Spectrometric Analysis of Eight Common Chemical Explosives Using Ion Trap Mass Spectrometer. *Bull. Korean Chem. Soc.* **2013,***34*, 3659-3664.

(58) Borsdorf, H.; Mayer, T.Response of Halogenated Compounds in Ion Mobility Spectrometry Depending on Their Structural Features. *Talanta,* **2011,***83*, 815-822.

Table of content

Formic Acid as a Dopant for Atmospheric Pressure Chemical Ionisation (APCI) for Negative Polarity of Ion Mobility Spectrometry and Mass Spectrometry

Vahideh Ilbeigi[1,*], Younes Valadbeigi[2], Ladislav Moravsky[1] and Štefan Matejčík[1,*]

[1]Department of Experimental Physics, Faculty of Mathematics, Physics and Informatics, Comenius University in Bratislava, Mlynská dolina F2, 84248 Bratislava, Slovakia.

[2]Department of Chemistry, Faculty of Science, Imam Khomeini International University, Qazvin, Iran.

Emails: vahideh.ilbeigi@fmph.uniba.sk; stefan.matejcik@fmph.uniba.sk